33RD CONGRESS
OF THE INTERNATIONAL COUNCIL
OF THE AERONAUTICAL SCIENCES
STOCKHOLM, SWEDEN, 4-9 SEPTEMBER, 2022

ICAS 2022 SWEDEN

IMPLEMENTATION OF WING ICE PROTECTION SYSTEM IN MORE ELECTRIC AIRCRAFT TECHNOLOGIES

Dhruv Haldar[1], Emil Holmgren[2] & Andreas Johansson[34]
[1]KTH Royal Institute of Technology, Stockholm, Sweden
[2]KTH Royal Institute of Technology, Stockholm, Sweden
[3]School of Electrical Engineering and Computer Science (EECS), KTH Royal Institute of Technology, Sweden
[4]SAAB AB, Linköping, Sweden

Abstract

More Electric Aircraft (MEA) technologies aim at reducing greenhouse gas emissions to make local and global air transport easier [6], while at the same time being cost-effective, reliable and promoting the production of more energy-efficient vehicles. The primary goal of this research is, therefore, to establish a framework for determining whether MEA technology applied to a specific aircraft subsystem will be useful. Goal of this paper is the development of a tool that can assist in evaluating the Wing Ice Protection System (WIPS) fuel consumption of MEA airliners of any size and flight. A method is provided for calculating the mass of ice formed when an Airbus A320 aircraft is subjected to a series of in-flight icing conditions during Climb and Descent. These in-flight icing conditions consist of humidity due to precipitation, and the air temperatures lying between the freezing ranges of 273.15 K to 253.15 K. The case study used in this paper modifies the existing study by using an icing air temperature of 256 K and an icing duration of 130.5 seconds for the Climb Case and 151.5 seconds for the Descent Case. The study utilizes publicly available aircraft data and Appendix C, CS-25 EASA icing aviation standards [6]. Power and fuel consumption of conventional Wing Ice Protection System (p-WIPS) and electro thermal Wing Ice Protection System (e-WIPS) was computed. Results revealed a significant reduction in e-WIPS power usage, ranging from 13% to 50% depending on the p-WIPS configuration chosen.

ICAS topic area: Hybrid/Electric and Unconventional Fuel Aircraft.

Keywords: Fuel consumption, Mass of Ice, More Electric Aircraft, WIPS, FENSAP-ICE.

1. General Introduction

1.1 Context

As the world's population grows, so does the number of people who travel around the world. The aviation industry is compelled to create more fuel efficient vehicles. Advisory Council for Aeronautics Research in Europe (ACARE) has set several targets to be accomplished by 2050 for air transport [3]. Some of the goals proposed are 75% reduction in CO2 emissions per passenger kilometre, a 90% reduction in nitrogen oxide (NOx) emissions and perceived noise emittance of aircraft by 65% by 2050 [3].

Collaboration between corporations, research institutes, and universities is becoming increasingly important in order to attain these targets. Swedavia, which owns and operates Sweden's busiest airports [9], proposed a new aviation strategy in 2020 which focuses on the development of electric and more-electric architectures and the required necessary infrastructure by 2025 [8]. The policies provided by the government and corporations instill confidence in the use of MEA Technologies.

1.2 Motivation

In partnership with SAAB AB Linköping, Sweden the RCAM research group at KTH, Stockholm, Sweden conducted a previous MEA investigation. The outcome from the MEA study done by Yidiz [5], in which a passenger aircraft comparable in size to the Airbus A320 was used, provided a basis for starting this paper.

2. Ice Protection System (IPS)

2.1 Mechanism of Ice Protection

In certain situations, snow and ice protection can also be provided to the aircraft when it is not in flight (or grounded) by spraying Type I Fluid diluted with water. The Type I fluid consists of propylene glycol, which is heated to a temperature of 60°C to 65°C. The system that operates to remove ice buildupis called a de-icing system. In contrast, the system used to avoid ice buildup formation is calledan anti-icing system. For the anti-icing system, the fluid used is Type IV, which is a more viscous version of Type I, not mixed with water. Propylene glycol is non-toxic, whereas Ethylene glycol, another lesser-known substance used, is toxic. The pilots disable the aircraft's ventilation system to prevent fluid fumes from entering inside during the application of Type I and Type IV Fluids. Type IV fluids gradually lose effectiveness during flight, and this is where the standard electrothermal andpneumatic ice protection systems come into play [1]. Thermal IPS constitute one of the most common systems used for aircraft surfaces vulnerable to ice build-up. The IPS systems operate in Running-wet air mode that amplifies the energy demand [2]. In the running-wet mode, the temperature of the contact region has to be higher than 0°C thereby maintaining a heavy dependency on the ambient climate temperature, normally between 0.6°C and 7.2°C, and this results in a very high power demand of 16.4 kW to 26.4 kW/m^2.

2.2 Icing Standards

The IPS must certify airworthiness requirements for flights into icing conditions. At present, the safety regulation is pursuant to Appendix C [13], Amendment 24, CS-25 of European Union Safety Agency (EASA) ED Decision 2020/001/R. The primary objective of Appendix C is to provide the highest possible (99%) icing conditions that the IPS should endure. According to Appendix C Part 1, for a non standard horizontal extent, the LWC is calculated by multiplying the LWC values of standard horizontal extent, by the Liquid Water Content factor F corresponding to the non-standard horizontal extent. Appendix O provides the data for calculating the LWC for a non-standard horizontal extent subject to freezing rain and freezing drizzle conditions.

2.3 IPS Function

The function of the IPS is to provide ice protection to various crucial components that come directly in contact with ice, be it during flight or when the aircraft is on the ground. For MEA technologies, the need to incorporate the IPS arises from the fact that IPS plays a significant role in electrical power consumption [10]. IPS functions either in Anti-icing or De-icing mode. In Anti-icing, the system functions continuously or in intervals. In contrast, the system is used only when the ice accretion passes a pre-determined threshold in the de-icing method.

Current IPS research is focused mostly on Wings (WIPS) and Cowl (CIPS). This study focuses only on WIPS. WIPS focuses on the ice protection of the leading edges of the aircraft wings. Wing de-icing is normally performed by hot bleed air coming from the engines on a large airplane, i.e., the system is pneumatic. However, electrical power is utilized for heating coils/pads used for anti-icing purposes.

2.4 Conventional/Pneumatic Evaporative Wing Anti-icing system (p-WIPS)

Bleed air from the engines is passed to the inner airfoil surface via the piccolo tube. Due to the heat flux associated with the conduction of Piccolo tube, the outer airfoil surface heats up and melts the ice. The major disadvantage of using this system is that it adversely affects the engine performance.

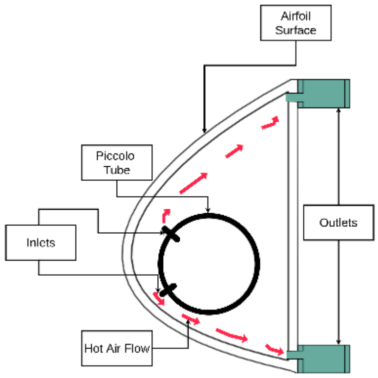

Figure 1 – p-WIPS.

System works in cycles of ON-OFF states. There is a simple empirical equation 1.1 to calculate the power requirements for anti-icing p-WIPS system. From that equation, the power requirements for deicing are calculated based on experimental evidence which shows that de-icing is approximately 25% to 35% of the power which is required for anti-icing [24], the same is represented in 1.1.

$$P_{p\text{-}WIPS,Anti\text{-}icing} = c_{p,AI} * \dot{m}_{WIPS\ ON,OFF} * (T_{WIPS} - T_{slat,surface}) * \eta_{p\text{-}WIPS} \quad (1.1)$$

In Equation 1.1, the variable $c_{p,AI}$ refers to the specific heat capacity of Air in anti-icing; $\dot{m}_{WIPS\ ON,OFF}$ is the mass flow rate of airflow from pneumatic inlets to top and bottom outlets; the variable T_{WIPS} is the temperature of the internal airflow. The variable $T_{slat,surface}$ refers to how much the temperature should be on the protected (or slat) surface so that all of the ice which is on the surface, melts completely.

$$P_{p\text{-}WIPS,De\text{-}icing} = 0.30 * P_{p\text{-}WIPS,Anti\text{-}icing} \quad (1.2)$$

Since the system works in ON and OFF states, the values of the variable $\dot{m}_{WIPS\ ON,OFF}$ keeps changing. The bleed air comes from two sources, namely the Engine and Auxilliary Power Unit (APU). The OFF state is characterized by the engine bleed air, with no bleed air coming from the APU. Subsequently the ON state is characterized by bleed air coming from the APU compressor along with the engine bleed air. Taking values of $\dot{m}_{WIPS\ ON,OFF}$ from Figure 4.15 (a) Liscouët-Hanke [11] because the initial configuration of [11] is similiar to the Climb and Descent Case study using Airbus A320. From experimental results and historical performance [11], the efficiency of using p-WIPS represented by $\eta_{p\text{-}WIPS}$ was computed to be approximately 65%.

Parameter/Variable	Value	Unit
$\dot{m}_{WIPS\ ON}$	0.8	kg/s
$\dot{m}_{WIPS\ OFF}$	0.6	kg/s
$c_{p,AI}$	900	J/Kg/K
$\eta_{p\text{-}WIPS}$	0.65	-

Table 1 – Parameters of Equation 1.1.

2.5 Electrothermal Running-wet Wing anti-icing system (e-WIPS)

In this system, the outer airfoil surface has slabs of various materials, electric power provided heats those materials and melts the ice. The airflow domains are separated from the metal or composite skin of the aircraft component; therefore, all the ANSYS airflow solvers can be used. Figure 2 shows how the heating pads are attached below the slat surface. For e-WIPS, the IPS response time to the cyclic activation of heater pads is analyzed in a time-dependent CHT simulation encompassing phase change, heat conduction and water runback to accurately predict the amount of ice that forms, melts and refreezes.

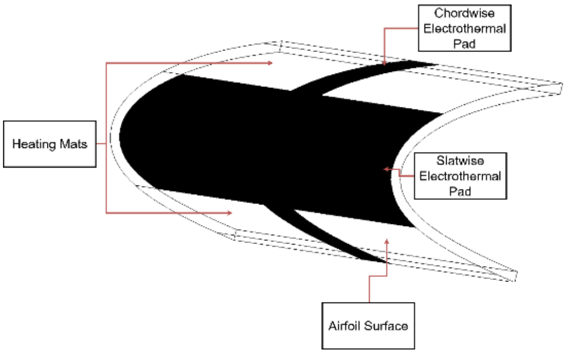

Figure 2 – e-WIPS.

Heat flux is implemented to the protected surface using the heating pads. Heating pads are placed inside the slat surface, or the surface where there is the most possibility of icing, in case of airfoil, it refers to the leading edge. Function of the heating pads is to evaporate the falling water droplets, preventing dangerous ice accumulation on the wings. There are different ways to implement e-WIPS, it can be done using solenoid actuators (for de-icing), electromechanical actuators, or electrothermal heating pads. In this study, simulation was performed on electrothermal heating pads. Equation 4.11 of Hanke [11] further states that in case of heating pads, the efficiency of an e-WIPS is 0.9 times than that of p-WIPS.

$$P_{e\text{-}WIPS,Anti\text{-}icing} = 0.90 * P_{p\text{-}WIPS,Anti\text{-}icing} \quad (2.1)$$

$$P_{e\text{-}WIPS,De\text{-}icing} = 0.90 * P_{e\text{-}WIPS,Anti\text{-}icing} \quad (2.2)$$

Relation between mass of ice and calculation of IPS Electrothermal power utilization is represented by Equation 2.3. SA_{wing} refers to the surface area of wing calculated from geometry used for the simulation. $\varsigma_{slat,wing}$ is ratio of slat (active surface where the heater will work) and wing surface. $TE_{heatice}$ refers to the energy required to heat ice to 0 degrees Celsius. $TE_{meltice}$ is the energy required to melt ice at 0 degrees Celsius. $TE_{heatwater}$ refers to the energy required to heat water to 10 degrees Celsius. $Cp_{ice\text{-}14,0}$ and $Cp_{ice0,10}$ refer to the specific heat capacity of ice and water. Variable L_{heat} refers to the Latent heat of ice. The equation 2.5 refers to the fuel consumption in kg. In equation 2.5, the variable TSFC refers to the Thrust Specific Fuel Consumption [12] parameter which is dependent on engine type and is a function of Mach number and temperature. kP refers to the shaft power factor [12] which is dependent on engine type and is a function of Mach and altitude. P_W is the power in watts. t_{icing} is the time of ice formation.

$$\varsigma_{slat,chord} * \varsigma_{slat,wing} * SA_{wing} * Mass_{ice} (Cp_{ice\text{-}14,0} + L_{heat} + Cp_{ice0,10}) = TE_{heatice} + TE_{meltice} + TE_{heatwater} \quad (2.3)$$

$$P_W = (TE_{heatice} + TE_{meltice} + TE_{heatwater}) / t_{icing} \quad (2.4)$$

$$Fuel = (kP)*(TSFC)*(P_W)*t_{icing} \quad (2.5)$$

Parameter/Variable	Value	Unit
SA_{wing}	122.6	m^2
$\varsigma_{slat,wing}$	0.78	-
$\varsigma_{slat,chord}$	0.15459	-
$Cp_{ice\text{-}14,0}$	2108	J/kgK
$Cp_{ice0,10}$	4179.6	J/kgK
$TE_{heatice}$	479769.5011	J
$TE_{meltiice}$	4471565.28	J

$TE_{heatwater}$	559561.5043		J
kP	2.07E-03 (Climb)	1.93E-03 (Descent)	N/W
$TSFC$	1.7659E-05 (Climb)	1.81E-05 (Descent)	kg/Ns

Table 2 – Parameters of Equation 2.3 and 2.5.

3. Methodology

3.1 Model Selection Methodology

The design and utilization of a mathematical model to simulate effects of turbulence constitute the initial stages of icing simulation. In most real-life scenarios, the boundary layer and wakes formed around the airplane wing are turbulent. Some of the observable effects of turbulent fluid flow are diffusiveness, dissipativeness, inconsistency and continuousness formed by tiny eddies [15].

3.1.1 Rationale and Motivation for model selection

It has been observed from a large number of experiments that the Spalart-Allmaras Turbulence Model (SPT) [16] solutions converge much faster and simpler than the k-omega SST Turbulence Model (ko-SST) [18] since only one computation of the transport equation is performed in SPT. Values for adjustable constants used in all of the three models are produced after data-fitting an extensive range of free turbulent flows. k-epsilon Turbulence Model (k-ET) [17] is not suitable for near-wall treatment. Due to the implementation of Shear Stress transport equation, ko-SST provides better implementation and prediction of complex flow separation and enhanced near-wall treatment. Another significant advantage is its high precision to cost ratio. Additionally, ko-SST offers highly accurate velocity profiles. ko-SST is the most popular model in the industry, and all of the reasons provide significant confidence to select ko-SST as our go-to model. In addition to ko-SST, SPT was implemented through FENSAP-ICE since it supports only SPT.

3.2 Software Selection Methodology

A great benefit of using this methodology is that it offers an option for automation of the airfoil geometry creation using IronPython programming [23]. Airfoil related parameters such as Angle of attack (AoA), type of airfoil and number of points (NumPoints) were fed into a MATLAB [27] code.

Additionally, the MATLAB code contained commonly used airfoils from the UIUC airfoil coordinate database [7]. Output from the MATLAB code was then integrated to script the airfoil geometry using ANSYS SpaceClaim. The airfoil geometry was then meshed and further icing simulation was performed within ANSYS. Icing related parameters such as Atmospheric reference conditions (Air Velocity, Droplet Diameter, Reynolds Number, Mach Number), Ice Type, Ice Density, Turbulence Model, Cloud type, Time of Icing formation and Liquid Water Content are implemented and simulated using ANSYS FENSAP-ICE [4].

Icing-related results include parameters such as Mass of Ice, Langmuir D Distribution, Change in Water Film Thickness, Change in Instantaneous Ice Growth, Mass Inflow, Mass Outflow, Mass Deficit and the shape of Icing formed obtained from the ANSYS FENSAP-ICE simulation.

3.2.1 Rationale and Motivation for software selection

It is essential that students and researchers should be able to repeat the conditions described in this study to get the same results. The ANSYS SpaceClaim and ANSYS FENSAP-ICE software package available is currently in bleeding-edge status. However, both help us to attain the objective within respectable assumptions using standard mathematical models. Additionally, ANSYS FENSAP-ICE is the only software that has an extensive set of features necessary for IPS. The openness and the advantages of FENSAP-ICE make it a suitable candidate to simulate our case study.

3.2.2 Workflow automation using Ironpython scripting in ANSYS SpaceClaim

In ANSYS SpaceClaim [26] , there are two methods for automating the geometry. The first is through blocks, and the second is through script. The main benefit of using SpaceClaim scripting is that it simplifies the development and repetition of basic geometry-related tasks and simplifies the creation and repetition of complex workflows. The compiler runs on an open-source language called

IronPython. IronPython provides a bridge between the Windows .Net Framework and Python libraries [23]. The automation code written for this study was compiled using the latest V20 Beta API.
By default, the IronPython SpaceClaim scripting is only capable of creating geometry. However, there was a choice to allow meshing automation inside SpaceClaim. The SpaceClaim meshing method had very limited and basic features, as it was meant for simpler objects (geometries). The command *SetFaceMeshTypeOptions()* was used to enable meshing and set the meshing options supported in the ANSYS Meshing software (separate software package inside ANSYS). The *SetFaceMeshTypeOptions()* command seemed to work in the initial iteration of geometries made. However, since the SpaceClaim mesh compiler was bleeding-edge, the compiler kept on crashing. This became more prevalent as the newer iterations made the airfoil geometry more complicated. Hence, the utilization of SpaceClaim scripting for meshing automation was dropped. However, the compiler should work fine as the product gets developed in further releases of the ANSYS Software package.

4. Icing Simulation

4.1 Climb Input Parameters

Parameter	Value		Unit
Temperature at Sea Level	288.15		K
Pressure at Sea Level	101325		Pa
Altitude	19685.04		ft
Altitude	6000		m
Air static pressure at altitude	47217.45		Pa
Droplet Diameter	20		microns
Droplet Distribution	Langmuir D		
Air Velocity	120		m/s
Aircraft Speed	190.25		m/s
Icing air Temperature	256		K
Icing Duration	130.5		seconds
Clouds	Stratiform	Cumuliform	-
Ice Type	Rime	Glaze Advanced	-

Table 3 – Climb Input Parameters.

4.2 Descent Input Parameters

Parameter	Value		Unit
Temperature at Sea Level	288.15		K
Pressure at Sea Level	101325		Pa
Altitude	19685.04		ft
Altitude	6000		m
Air static pressure at altitude	48974.5		Pa
Droplet Diameter	20		microns
Droplet Distribution	Langmuir D		
Air Velocity	120		m/s
Aircraft Speed	202.75		m/s
Icing air Temperature	256		K
Icing Duration	151.5		seconds
Clouds	Stratiform	Cumuliform	-
Ice Type	Rime	Glaze Advanced	-

Table 4 – Descent Input Parameters.

4.3 Langmuir D distribution

Langmuir D Distribution of droplets with Median Volume Diameter (MVD) 20 μm is used for the study. The distribution contains a set of seven ratios of diameters corresponding to the percentage of Liquid Water Content (LWC). For a given MVD, there are seven values in a Langmuir D distribution. In the past, NASA has used distributions published by Langmuir to assess MVD that are now in Appendix C [13]. The upper limit for Langmuir- D distribution is an MVD of 50 μm. Figure 7 and 8 depict the LWC and Collection efficiency for 7-diameter Langmuir-D distributions. The dashed line represents the final solution generated using weights on each droplet size. Figure 3 shows the diameters corresponding to Langmuir D distribution.

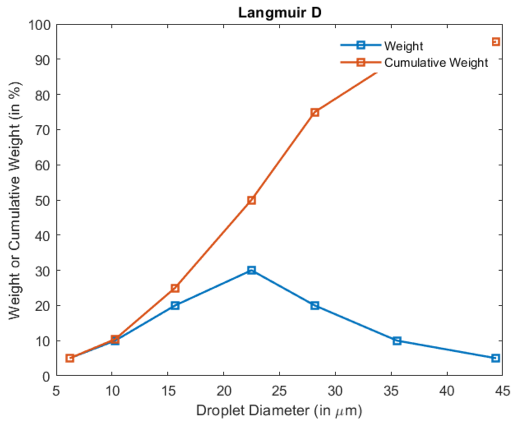

Figure 3 – Langmuir D Distribution Diameters.

4.4. Simulating the Icing Parameters

The physics and thermodynamics of in-flight icing are based on strong heat convection in fluids. IPS simulations are far too complicated to be handled in a single computational domain. Applying a divide and conquer strategy, which involves computing the solutions of the different domains separately and exchanging interface boundary conditions in an iterative manner, is the most computationally efficient option. Heat fluxes and temperatures are equalized across interfaces to achieve convergence. The simulation is divided to multiple domains (or iterations), data computed from previous domain gets carried forward to the next, and so on. These iterative simulations are discussed with the results in detail in Sections 5.1 to 5.3 of this paper.

ANSYS OPTIGRID performs anisotropic mesh optimization. The way it works is, that it first estimates the difference or error *e(x)* between the exact solution *f(x)* and numerical solution $f^{num}(x)$ of a given flow problem of a specified grid size *S(num)*. This error *e(x)* can come from a variety from sources, such as arising from approximations of geometric solid boundaries, rounding off, damping, insufficient flow solver convergence and inadequate grid distribution [28].

Figure 4 shows that failed methods were primarily due to software incompatibilities and a lack of a simpler approach. Gmsh [29] also had mesh scripting automation however it was discontinued in favor of ANSYS, which had more integration with the latter parts of the approach used in the study.

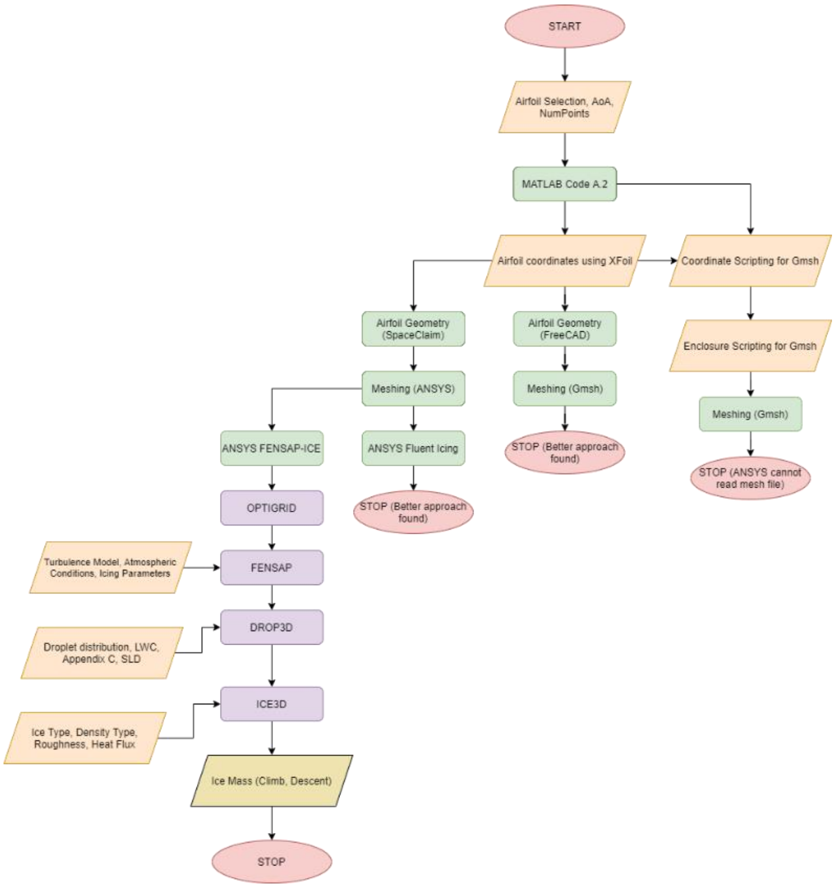

Figure 4 – Flowchart of Icing Parameters Simulation showing failed and successful methods.

5. Results

The icing simulation occurred for a total duration t_{icing} of 130.5 and 151.5 seconds for Climb and Descent Cases. Droplet parameters were conformant to the conditions as specified in Appendix C [13] forming Continuous maximum or Stratiform clouds. Three iterative steps of the icing simulations were repeated for both Climb and Descent Study cases.

5.1 Icing Parameters simulation using FENSAP

The first step of this iterative simulation involves computing for the icing airflow. The optimized grid file generated from OPTIGRID was input at this stage. The physical model in FENSAP was selected as Air following by selection of the Navier-Stokes momentum equation and the Full PDE Energy equation and SPT Turbulence model. Global Parameters for solver such as the CFL number and maximum number of timesteps were input. The global parameters get carried forward as the file goes through iterative simulations. The optimized mesh can be observed in Figure 5.

Since the airfoil (or wall) is positioned within the Farfield enclosure, the wall distance increases as one moves away from the airfoil and towards the enclosure boundaries. On the airfoil surface, a no-slip wall boundary is applied. The same can be observed in Figure 6.

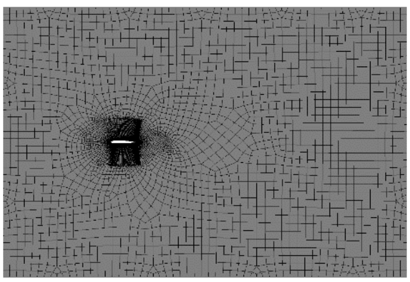

Figure 5 – Optimized mesh using OPTIGRID (2D view).

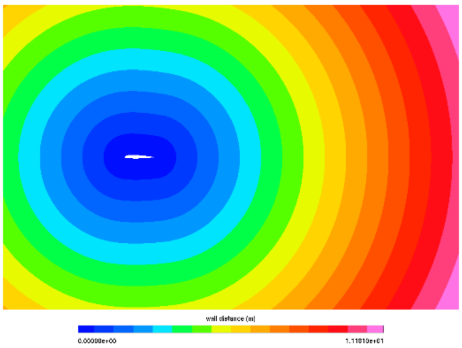

Figure 6 – Wall Distance using FENSAP (2D view).

5.2 Icing Parameters simulation using DROP3D

The second step of the iteration deals with droplet impingement and crystal formation. For the sake of simplifying the scope of this paper; Supercooled Liquid Droplets, vapor model and crystal formations have been disabled. This step was repeated for Monodisperse (calculation for a single droplet diameter) and Langmuir D Distributions for both Climb and Descent cases. The boundary conditions were defined for subsonic flow.

Some of the input parameters were imported from the previous FENSAP step, and new ones added. They consist of the Appendix C implementation [6], Droplet Distribution, Particle Type and the Corrected LWC from Appendix C. The Corrected LWC was calculated by multiplying the original LWC by a factor which depends on cloud extent (32.375218 nautical miles), t_{icing} and air speed. **For the given reference parameters, the LWC factor came out to be 0.7791475**.

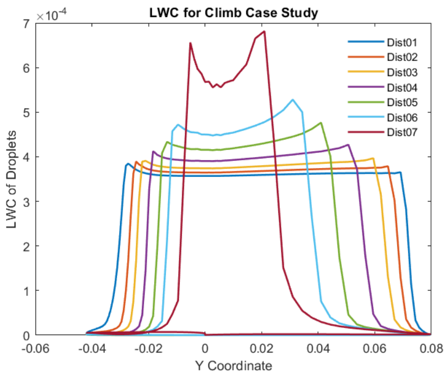

(a)

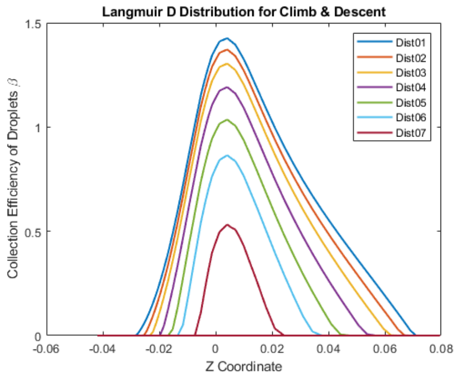

(b)

Figure 7 – (a) LWC (b) Collection efficiency for Langmuir D Distribution using DROP3D.

In Figure 7(a), smallest droplet size corresponds to the curve with the lowest beta, and the largest droplet size corresponds to the curve with the largest beta. Smaller droplets are less ballistic, tending to follow the air flow to escape jets, lowering collection efficiency and droplet impingement limits. Larger droplets are more ballistic and do not suit the airflow as well. As a result, they have a higher collection efficiency and impingement than the smallest droplets. In general, this detail is critical for correctly designing the IPS power and coverage specifications.

From Figure 7(b), it is observed that the maximal beta exists at the stagnation point, which in this situation is just below the leading airfoil edge. The limits of droplet impingement are the points on the upper and lower surfaces where the beta becomes zero. Since any of the water that impinges is immediately frozen in rime icing situations, the maximum extent of icing is equal to the impingement limits. Water will runback and freeze beyond the impingement limits in glaze icing. The maximum beta is normally less than 1.0, and as the droplet flow becomes tangent to the surface, the beta decreases.

5.3 Icing Parameters simulation using ICE3D

The third and final stage of the iterative simulation involves the computation of icing-related parameters. This step was repeated for Rime and Glaze Type ice formation scenarios. The input parameters which were added from scratch include the Ice-Water Model, Skin Emissivity, Recovery Factor (should have a value between 10 and 20, 20 was chosen), and automatic Timestep (based on icing time of 130.5 and 151.5 s). The output parameters obtained were the Ice Shape, Total Mass of Ice, Change in Instant Ice Growth, Change in Ice Surface Temperature and Change in Water Film thickness.

Observing the ice formation in Figure 8, **Ice is formed mostly on the airfoil leading edge**. As evident by Figure 10 (a), the change in water film thickness remains constant because of Rime ice formation. In the case of Figure 10 (b), however, it is observed that the water film thickness changes unevenly due to glaze ice formation,

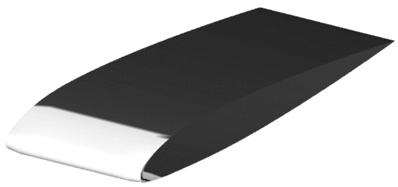

Figure 8 – 3D View of Rime Ice Accretion in Climb Rime case ICE3D.

(a) (b)

Figure 9 – Ice Shape formation for (a) Rime (b) Glaze Ice type using ICE3D.

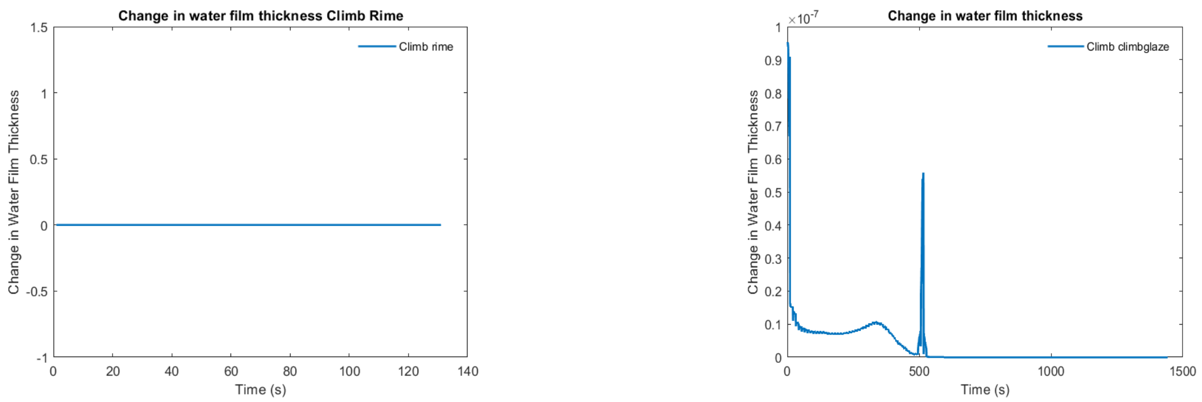

(a) (b)

Figure 10 – Change in water film thickness for (a) Rime (b) Glaze Ice type using ICE3D.

5.4 p-WIPS Results

To properly understand the p-WIPS airflow, the temperature is represented in 3.1 by the T_{WIPS} variable. The two configurations or schemes for the p-WIPS were referenced from [19]. The first scheme has two inlets on cross-sections located away from the center. Subsequently, the second scheme has one inlet located on the middle of the cross-section. The pressure-type inlets in both the schemes are at a temperature of 453 K and have a gauge total pressure of 27600 Pa.
There are two walls: First wall is the outer surface of the airfoil, as that is where the icing phenomenon will occur. Consequently, the second wall is the total solid area of p-WIPS excluding the inlets and outlets. In the ANSYS FLUENT simulation, both the walls are thermally 'Coupled' meaning they undergo Conjugate Heat Transfer (CHT). The 'Coupled' boundary condition regulates thermal energy on both sides of the walls simultaneously.
For both the schemes, the two outlets are located away from the leading edge of the airfoil in top and bottom positions. The pressure-based outlets have a pressure of 55676 Pa and have a total backflow temperature of 300 K. Thus, the jet of bleeding air from the inlets warms the outer airfoil surface which is thermally coupled, and flows internally towards the outlets.
After substituting the values T_{WIPS} and air mass flow rate $\dot{m}_{WIPS\ ON,OFF}$ in the computation of Equation 1.1, the **total power utilization of p-WIPS came out to be 64.51 kW (ON state), and 48.38 kW (OFF state)**.

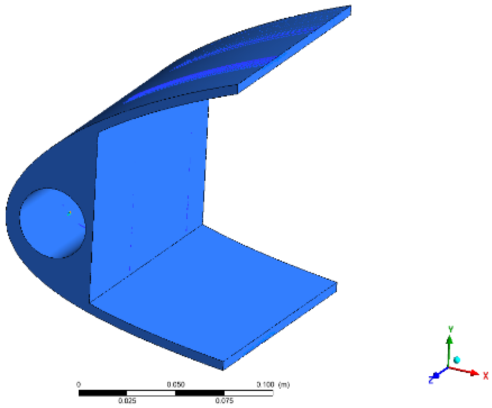

Figure 11 – Piccolo Tube Geometry.

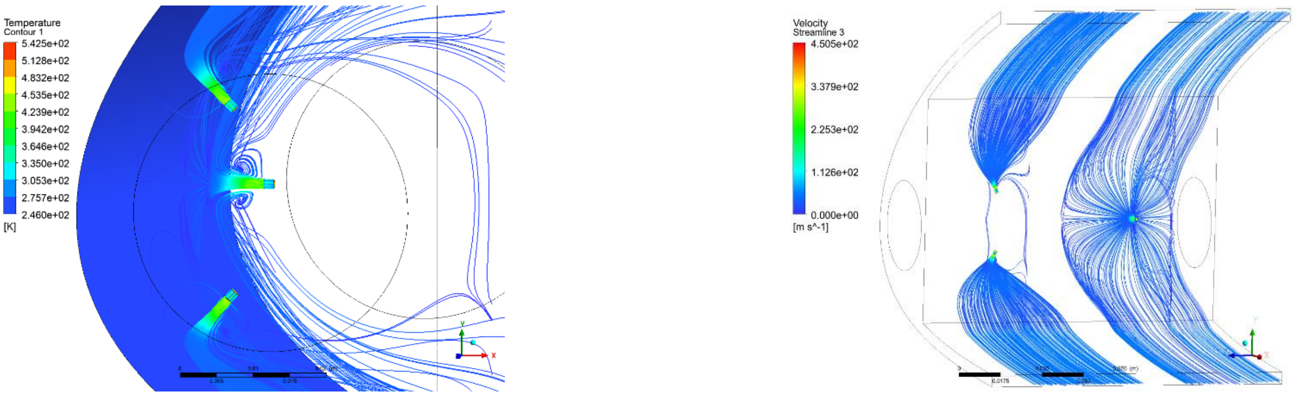

(a) (b)

Figure 12 – Velocity vectors for p-WIPS using ANSYS FLUENT.

Two Planes were created in the post simulation phase in order to see the airflow vectors in the internal region of the p-WIPS. These Planes were created corresponding to the two different schemes which were used in this analysis, the same can be observed in 13 (a). Upon close observation of Figure 12 (b) and 13 (b), it is observed that Eddies are formed on the corners of the p-WIPS and on the inlets.

5.5 e-WIPS Results

To properly understand the Electrothermal heating pad-mat based icing systems, two separate simulations were performed to view temperature and heat flux distribution according to the reference values from Peng et al [20].

Scheme 1 consisted of cross-pads which divided the icing surface into four heating mats in quadrant form. For Scheme 1, the cross-heater pad is at a temperature of 299 K. Scheme 2 consisted of heating pads which divided the icing surface spanwise. The heating pads are also referred to as parting strips in some of the articles used for referencing [21].

Looking at the contours at Figure 13 and 15, we observe that the heater pad is coupled to the icing surface leading to a phase of transient heat transfer. Temperature of 303.15 K or 30 degrees Celsius was applied to the heating mats in both the schemes, since most IPS require temperatures ranging from 283.15 K and a maximum of 308.15 K for full ice removal from wing surface [22].

Equation 2.3 was computed in order to obtain the power and fuel consumption for w-WIPS Simulation. **The total power utilization of e-WIPS came out to be 42.23 kW for the climb case, giving a fuel consumption of 0.201 kg. For the descent case, power utilization was 43.2 kW, with a fuel consumption of 0.228 kg.**

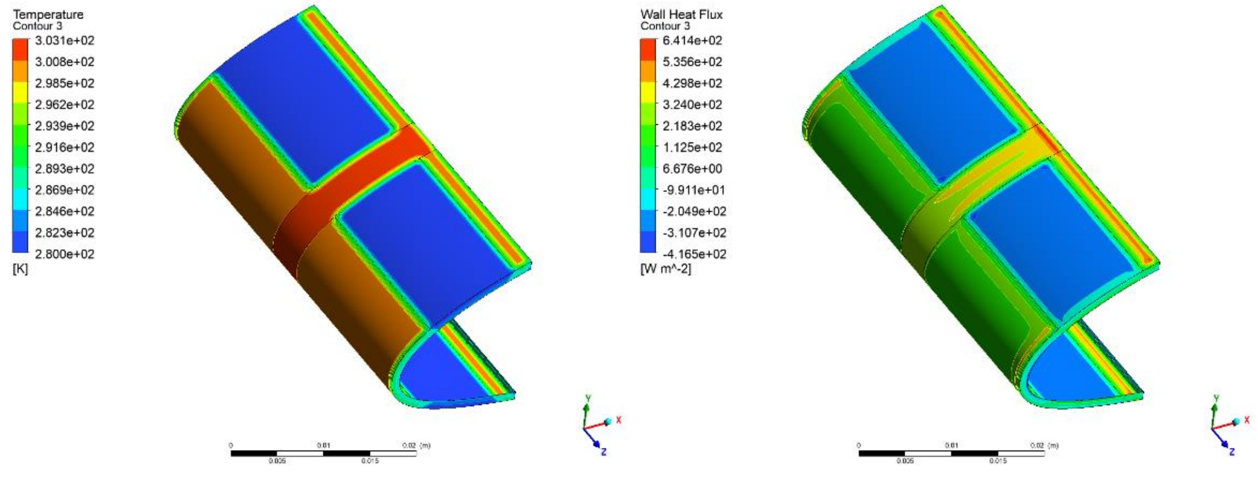

(a) (b)

Figure 13 – (a) Temperature (b) Heat Flux distribution in Scheme 1 of e-WIPS.

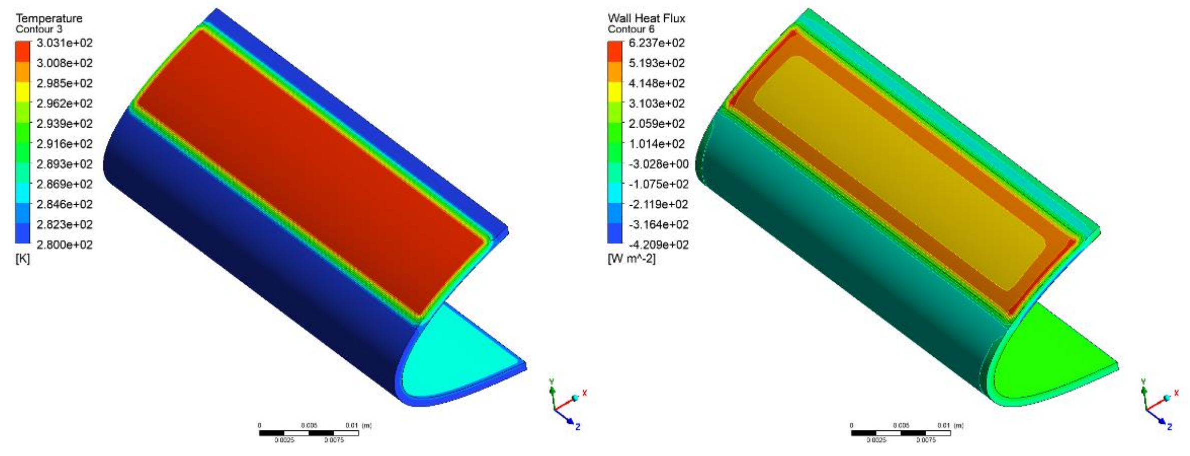

(a) (b)

Figure 14 – (a) Temperature (b) Heat Flux distribution in Scheme 2 of e-WIPS.

6. Icing Validity Analysis

This section tries to answer the question, How do we know if this method is valid and robust? The primary objective of validation analysis is for applying the developed model to different aircraft types, and test it accordingly.

NACA 0012 is a 4-digit series airfoil originally mathematically designed from desired lift characteristics. The Validation study was carried out using the reference conditions and input parameters shown in Figure 6 (e), Page 10 of Shin et al [14] for icing on a NACA 0012 airfoil. Table 5 contains a list of the input parameters. The motivation for selecting the parameters stems from the fact that these parameters apply to all types of ice: Rime, Glaze, and Transition 2.2, as stated on Page 5 of [14].

The experimental data of the ice shape was obtained from NASA Lewis Icing Research Tunnel (IRT). The IRT has a test section of 1.8288 m in height, 2.7432 m in width and 6 m in length. However, since the ice shape created during the Shin et al experiment is based on chord length ratios, the ice shape formation should be the same regardless of chord length. The Figure 15 shows the ice shape formation on NACA 0012 airfoil. During the Shin et Al experimental analysis, Liquid Water Content and Median Volumetric Diameter were controlled by the icing sprays.

Shin et al used a NACA 0012 test model of 1.8288 m height and 0.5334 m chord length. Contrastingly, the dimensions for the FENSAP-ICE simulation are 1.0084 m span, 0.1 m chord length which is including the closed trailing edge. **Observing Figure 15 (a) and (b), the ice shape formations from the analysis came out to be reasonably similiar as Figure 6 of Shin et al [14] giving a total mass of ice as 0.429 kg.**

Property	Value	Unit
LWC	1	g/m^3
Air Speed	67.05	m/s
Angle of Attack	4	Degrees
Icing Time	360	s
Median Volumetric Diameter	20	μm
Icing Air Temperature	247.03	K

Table 5 – Validity Analysis using NACA 0012.

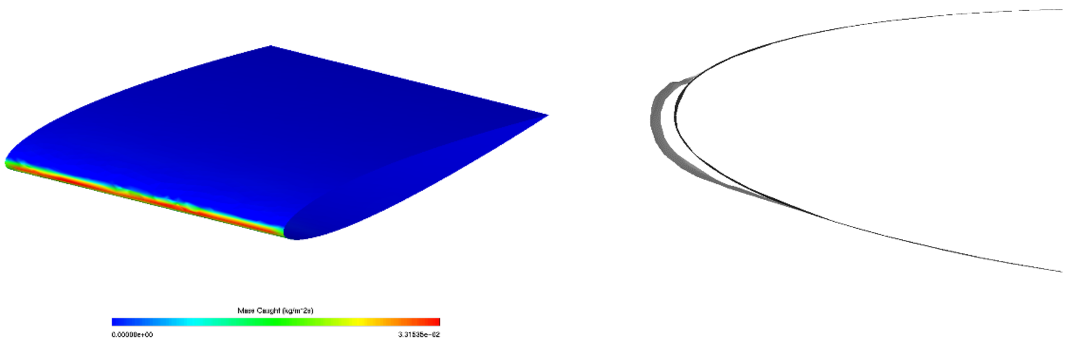

(a) (b)

Figure 15 – (a) 3D view (b) 2D view of mass caught in NACA 0012 using Validation Parameters in ICE3D.

7. Conclusion

Implementation of the electrothermal system is one of the ways that More Electric Aircraft technologies can be used in order to meet future environmental goals. There exists a significant reduction in power consumption when going forward with MEA Technologies for IPS. Weight poses a significant threat to MEA Technologies, and is directly dependent to the development of Power Electronics and Battery industry [24]. Future application for this approach includes the implementation of Cowl Ice Protection System (CIPS), Wind Turbine icing approximation. MEA Technologies could potentially be utilized to power secondary subsystems present in the aircraft such as landing gear, Environmental Control System (ECS). The opportunity for investigation is not limited to aircraft subsystems, but also includes ground systems. Wirén [25] from the EECS department at KTH proposed the feasibility of replacement of conventional ground vehicles with alternative electric vehicles.

The presented research work suggests a methodology based on an automated and robust approach that introduces the capability to implement icing phenomenon of aircraft. The power consumption of the Electrothermal Wing Ice Protection System and Pneumatic Wing Ice Protection System is in conjunction to the real-world consumption parameters. The icing conditions and parameters conform to the strict laws and standards established by aviation authorities around the world.

The approach has a significant disadvantage in that it is dependent on commercial software packages. Furthermore, there is a scarcity of publicly available data that could have improved the results presented in this paper. If I had to do the research work again, I would have taken a more practical and top-down approach and attempted to improve on the failed approaches mentioned in Figure 4.

8. Acknowledgement

Prof. Lina Bertling Tjernberg is a professor at the KTH Royal Institute of Technology's School of Electrical Engineering and Computer Science. She assisted me in asking the research questions related to MEA Technologies and is actively involved in its development.

9. Contact Author Email Address

Name: Dhruv Haldar
Email: haldardhruv@gmail.com, haldar@kth.se

10. Copyright Statement

11. References

[1] Mike Arnot. *How Aircraft De-Icing Works*. 2018. URL: https://thepointsguy.com/news/ how-aircraft-de-icing-works/(visited on 01/30/2021).

[2] N.A. *Assessment of Effects of Mixed-Phase Icing Conditions on Thermal Ice Protection Systems*. Tech. rep. 2003.

[3] M Dareck, C Edelstenn, and T Ender. *Flightpath 2050 Europe's Vision for Aviation*. Tech. rep. 2011, p. 28. DOI: 10.2777/50266. URL: http://ec.europa.eu/transport/modes/ air/doc/flightpath2050.pdf.

[4] Wagdi G. Habashi et al. "Fensap-Ice : a Fully-3D in-Flight Icing Simulation System for Aircraft, Rotorcraft and Uavs". In: *24th International Congress of the Aeronautical Sciences* (2004),pp. 1–10. URL: http://www.icas.org/ICAS_ARCHIVE/ICAS2004/PAPERS/608.PDF.

[5] Yildiz Mustafa. “On more electric airplane: case study Stockholm - Copenhagen”. MA thesis. 2019. URL: http://www.diva-portal.org/smash/get/diva2:1324716/FULLTEXT01.pdf.

[6] R. T. Naayagi. “A review of more electric aircraft technology”. In: *2013 International Conference on Energy Efficient Technologies for Sustainability*. Nagercoil: IEEE, Apr. 2013, pp. 750–753. ISBN: 9781467361507 9781467361491 9781467361484. DOI: 10.1109/ICEETS.2013. 6533478. URL: http://ieeexplore.ieee.org/document/6533478/.

[7] Michael S. Selig. *UIUC Airfoil Data Site*. 2012. URL: https://m-selig.ae.illinois. edu/ads/coord_database.html%20http://www.ae.illinois.edu/m-selig/ads/coord_database.html#N (visited on 02/24/2021).

[8] Swedavia. *Swedavia launches electric aviation strategy – Åre Östersund ready for first electric aircraftin autumn 2020 | About Swedavia*. 2020. URL: https://www.swedavia.com/about-swedavia/for-press/swedavia-launches-electric-aviation-strategy (visited on 05/06/2021).

[9] Wikipedia. *Swedavia - Wikipedia*. URL: https://en.wikipedia.org/wiki/Swedavia (visited on 05/06/2021).

[10] C. N. Donatti, R. A. Silveira, G. Bridi, C. R. Maliska, and A. F. C. Da Silva. “Ice Accretion Simulation in Presence of a Hot Air Anti-Icing System,” in *19th International Congress of Mechanical Engineering*, no. 1, p. 10. 2007.

[11] Liscouët-Hanke Susan. “A model-based methodology for integrated preliminary sizing and analysis of aircraft power system architectures,” Ph.D. dissertation, *Institut National des Sciences Appliquées de Toulouse*. [Online] 2008. Available: https://core.ac.uk/download/pdf/ 35285284.pdf

[12] Holmgren Emil. “MORE ELECTRIC AIRCRAFT (MEA) SCALING ASPECTS AND WEIGHT IMPACT” *33rd Congress of the International council of the aeronautical sciences*. Unpublished. 2022.

[13] European Aviation Safety Agency. “Certification Specifications and Acceptable Means of Compliance for Large Aeroplanes CS-25 : Amendment 24,” *European Union Aviation Safety Agency*. Tech. Rep. 2020.

[14] J. SHIN, T. BOND. “Results of an icing test on a NACA 0012 airfoil in the NASA Lewis Icing Research Tunnel” 1992. doi: 10.2514/6.1992-647

[15] Davidson. “Publication 97/2 An Introduction to Turbulence Models,” Tech. Rep., 2018. [Online]. Available: https://uu.diva-portal.org/smash/get/diva2:1038705/FULLTEXT01.pdf

[16] Langley Research Center, C. Rumsey. “Spalart-Allmaras Model,” pp. 1–3, 2015. [Online]. Available: https://turbmodels.larc.nasa.gov/spalart.html

[17] C. X. Zhang. “Numerical predictions of turbulent recirculating flows with a κ- model,” *Journal of Wind Engineering and Industrial Aerodynamics*, vol. 51, no. 2, pp. 177–201, 1994. doi: 10.1016/0167-6105(94)90003-5

[18] F. R. Menter, “Improved Two-Equation k-Turbulence Models for Aerodynamic Flows,” Tech. Rep., 1992.

[19] R. Hannat, F. Morency. “Numerical validation of CHT3D/CFX in anti-/de-icing piccolo system,” 4th AIAA Atmospheric and Space Environments Conference 2012, no. June, pp. 1–21, 2012. doi:10.2514/6.2012-2678

[20] L. Peng, K. Yuanli, S. Yupeng, and H. Xunan, “Transient simulation and analysis of wing electrothermal ice protection system,” *The Journal of Engineering*, vol. 2018, no. 13, pp. 438–445, 2018. doi:10.1049/joe.2018.0047

[21] O. Meier and D. Scholz, “A Handbook Method for the Estimation of Power Requirements for Electrical De-Icing Systems,” *Deutscher Luft-und Raumfahrt Kongress*, vol. 0, no. September, 2010. [Online]. Available: https://www.fzt.haw-hamburg.de/pers/Scholz/MOZART/ MOZART_PUB_DLRK_10-08-31.pdf

[22] X. Huang, N. Tepylo, V. Pommier-Budinger, M. Budinger, E. Bonaccurso, P. Villedieu, and L. Bennani, “A survey of icephobic coatings and their potential use in a hybrid coating/active ice protection system for aerospace applications,” Progress in Aerospace Sciences, vol 105, no. January, pp. 74–97, 2019. doi: 10.1016/j.paerosci.2019.01.002. [Online]. Available: https://doi.org/10.1016/j.paerosci.2019.01.002

[23] N. Foundation, “IronPython.net.” [Online]. Available: https: //ironpython.net

[24] Huang H. Challenges in More Electric Aircraft (MEA) - IEEE Transportation Electrification Community (Online). Retrieved from https://tec.ieee.org/newsletter/july-august-2015/challenges-in-more-electric-aircraft-mea, 2015.

[25] Wirén H. *Asset Management of Electrical Transportation Systems with Life Cycle Cost Analysis for Ground Support Equipment: Case Study Stockholm Arlanda Airport* (Dissertation). Retrieved Feb 2022, pp 1-83.

[26] ANSYS. “ANSYS SpaceClaim: 3D Modeling Software,” 2019. [Online]. Available: https://www.ansys.com/products/3d-design/ansys-spaceclaim

[27] Mathworks, “Simulink - Simulation and Model-Based Design - MATLAB Simulink,” 2020. [Online]. Available: https://se.mathworks.com/products/simulink.html

[28] ANSYS. *ANSYS FENSAP-ICE User Manual* Chapter 12. [Online]. Available: https://ansyshelp.ansys.com/

[29] C. Geuzaine, J.F. Remacle. “Gmsh: a three-dimensional finite element mesh generator with built-in pre-and post-processing facilities” Tech. Rep. 2009.